

# First Surface-resolved Results with the IOTA Imaging Interferometer: Detection of Asymmetries in AGB stars

Ragland, S.<sup>1,2</sup>, Traub, W.A.<sup>3,1</sup>, Berger, J.-P.<sup>4</sup>, Danchi, W.C.<sup>9</sup>, Monnier, J. D.<sup>6</sup>, Willson, L. A.<sup>11</sup>, Carleton, N. P.<sup>1</sup>, Lacasse, M. G.<sup>1</sup>, Millan-Gabet, R.<sup>5</sup>, Pedretti, E.<sup>6</sup>, Schloerb, F. P.<sup>7</sup>, Cotton, W. D.<sup>8</sup>, Townes, C.H.<sup>10</sup>, Brewer, M.<sup>7</sup>, Haguenaue, P.<sup>12</sup>, Kern, P.<sup>4</sup>, Labeye, P.<sup>13</sup>, Malbet, F.<sup>4</sup>, Malin, D.<sup>7</sup>, Pearlman, M.<sup>1</sup>, Perraut, K.<sup>7</sup>, Souccar, K.<sup>7</sup>, Wallace, G.<sup>7</sup>

## ABSTRACT

We have measured non-zero closure phases for about 29% of our sample of 56 nearby Asymptotic Giant Branch (AGB) stars, using the 3-telescope Infrared Optical Telescope Array (IOTA) interferometer at near-infrared wavelengths (H-band) and with angular resolutions in the range 5-10 milliarcseconds. These non-zero closure phases can only be generated by asymmetric brightness distributions of the target stars or their surroundings. We discuss how these results were

---

<sup>1</sup>Harvard-Smithsonian Center for Astrophysics, 60 Garden Street, Cambridge, MA 02138

<sup>2</sup>Presently at California Association for Research in Astronomy, 65-1120 Mamalahoa Hwy, Kamuela, HI 96743; sragland@keck.hawaii.edu

<sup>3</sup>Jet Propulsion Laboratory, M/S 301-451, 4800 Oak Grove Dr., Pasadena CA, 91109

<sup>4</sup>Laboratoire d'Astrophysique de Grenoble, 414 Rue de la Piscine, F-38400 Saint Martin d'Herès, France.

<sup>5</sup>Michelson Science Center, California Institute of Technology, Pasadena, 770 S. Wilson Ave., Pasadena, CA 91125

<sup>6</sup>University of Michigan at Ann Arbor, Department of Astronomy, 500 Church Street, Ann Arbor, MI 48109-1090.

<sup>7</sup>University of Massachusetts at Amherst, Department of Astronomy, LGRT-B 619E, 710 North Pleasant Street, Amherst, MA 01003-9305.

<sup>8</sup>National Radio Astronomy Observatory, 520 Edgemont Road, Charlottesville, VA 22903

<sup>9</sup>NASA Goddard Space Flight Center, Exoplanets & Stellar Astrophysics, Code 667, Greenbelt, MD 20771

<sup>10</sup>University of California at Berkeley, Space Science Laboratory, Berkeley, CA 94725-7450

<sup>11</sup>Department of Physics and Astronomy, Iowa State University, Ames IA 50014

<sup>12</sup>ALCATEL Space Industries, 100 boulevard du Midi, BP99, 06322 Cannes, France

<sup>13</sup>LETI, CEA-Grenoble, 17 rue des Martyrs, 38 054 Grenoble CEDEX 9, France

obtained, and how they might be interpreted in terms of structures on or near the target stars. We also report measured angular sizes and hypothesize that most Mira stars would show detectable asymmetry if observed with adequate angular resolution.

*Subject headings:* stars: AGB, stars: asymmetric stars, stars: circumstellar shell, stars: surface features, stars: non-radial pulsation, technique: long baseline interferometry, technique: closure phase

## 1. Introduction

The stars in this study are all AGB stars, that is, stars found at or near the tip of the Asymptotic Giant Branch in the HR diagram. They are low to intermediate mass stars, having already spent most of their lives as normal stars, and currently heading towards their deaths probably in the form of planetary nebulae, leaving the central star as a white dwarf. Most AGB stars are variable in brightness; those with relatively regular and large amplitude visual variations ( $> 2.5$  mag) with periods in the range 100 - 1000 days are classified as Mira variables. The Miras and some of the other, semi-regular (SR) or irregular (Irr) variables have observed mass loss rates ranging from  $10^{-7}$  to  $> 10^{-5} M_{\odot}$  per year (Knapp & Morris 1985). Diameter changes, opacity changes, and possibly other processes such as convection contribute to the brightness variation in these stars.

The Mira stage of evolution has been identified as marking the onset of the “superwind” phase, i.e. that evolutionary stage where mass loss rates rapidly increase and result in the termination of AGB evolution (Bowen & Willson 1991, Willson 2000). These stars thus serve as markers for the tip of the AGB in various populations, something already known for the shorter period cases from the few Miras that appear in globular clusters such as 47 Tuc (Frogel, Persson & Cohen 1981).

Miras with close companion white dwarfs usually are classified as symbiotic systems (Allen 1984; Whitelock 1987; Luthardt 1992; Belczyński et al. 2000). A few Miras are known to have companions but are not (or are only very mildly) symbiotic systems; this includes  $\alpha$  Cet = Mira, with a probable WD companion in a multi-century orbit (Reimers & Cassatella 1985; Wood & Karovska 2004). Statistics for the binarity of Miras are otherwise quite uncertain, in part because the expected orbital velocity amplitudes for a close companion, 30 km/s at 1 AU and 10 km/s around 5 AU, are very similar to the shock amplitudes of 20-30 km/s produced by the Mira pulsation itself (Hinkle, Scharlach & Hall 1984).

In this paper we use the word “asymmetry” to mean that part of the 2-dimensional

brightness distribution which cannot be made symmetric with respect to a reflection through a point. Thus, for example, an elliptical uniform disc or an equal-brightness binary system are both symmetric, but a binary with unequal brightness or a star with an off-centered bright/dark spot is asymmetric.

Departure from circular symmetry has been known in AGB stars from various high angular resolution observations (Karovska et al. 1991; Wilson et al. 1992; Haniff et al. 1992; Richichi et al. 1995; Ragland 1996; Weigelt et al. 1996; Karovska et al. 1997; Tuthill et al. 1997; Lattanzi et al. 1997; Wittkowski et al. 1998; Tuthill et al. 1999, 2000; Hofmann et al. 2000; Thompson et al. 2002; Monnier et al. 2004a; Weiner et al. 2006). The observed departures from circular symmetry have been interpreted either in terms of elliptical distortions or an otherwise symmetric photosphere containing localized compact features. However, no consensus exists as to the mechanism that would cause such departures from apparent circular symmetry.

Dust shells surrounding AGB stars have observed asymmetries as well such as in Mira (Lopez et al. 1997), the carbon stars IRC+10216 (CW Leo; Tuthill et al. (2000)), CIT 6 (Monnier, Tuthill & Danchi 2000) and IK Tau (Weiner et al. 2006) among others. The connection between apparent surface features and the morphology of the dust shells has not been established.

About 50% of all planetary nebulae (PN) display bipolar symmetry (Zuckerman & Aller 1986), but only a small fraction of circumstellar envelopes show bipolarity. A surprisingly large number of proto-PN show roughly circular arcs surrounding a bipolar core, suggesting that in most cases the AGB mass loss is spherically symmetric and the asymmetry seen in the PN occurs well after the Mira stage (Su 2004; Willson & Kim 2004). Recent studies of jets around a few AGB stars (Kellogg, Pedelty & Lyon 2001; Imai et al. 2002; Sahai et al. 2003; Sokoloski & Kenyon 2003; Brocksopp et al. 2004) from radio, x-ray or Hubble Space Telescope (HST) observations suggest that those stars showing substantial asymmetry may all have a low mass stellar companion accreting mass from the AGB primary. Recent SiO maser observations of AGB stars show departures from spherical symmetry (Diamond et al. (1994), Greenhill et al. (1995), Diamond & Kemball (2003), Cotton et al. (2004), Soria-Ruiz et al. (2004)). The observed circumstellar SiO masers tend to occur in clumpy, partial rings centered on the central star (Diamond et al. (1994)). Cotton et al. (2002) observed 9 stars in SiO, at least two of them known binaries, and used the modeling of Humphreys et al. (2002) in discussing the results. SiO maser emission comes from  $\sim 2\text{AU}$  or  $\sim 2R_*$  where the outflow velocity gradient along the line of sight is small. The special conditions required for maser emission potentially gives rise to bias in the statistics of asymmetry in the sample population of stars.

In this paper we report the initial results from one phase of a larger program, the Mira Imaging Project, to investigate asymmetries in AGB stars using three interferometer facilities, each capable of making closure phase measurements. These facilities are the IOTA, the Infrared Spatial Interferometer (ISI), and the Very Long Baseline Array (VLBA). The present paper focuses on IOTA results.

Subsequent to the work reported here, and as a part of the ongoing Mira Imaging Project, selected Mira targets with positive closure phase signal from our survey have been re-visited at different pulsational phases, baselines, position angles, and wavelengths in order to characterize the observed asymmetry. The results of this ongoing study will be presented elsewhere. In this article, we present the initial survey results for all our targets.

## 2. Observations

The observations reported here were carried out during the commissioning phase of the IOTA 3-telescope array (Traub et al. 2004) and integrated-optics beam-combiner, IONIC (Berger et al. 2004), operating in the H-band ( $1.65 \mu\text{m}$ ) atmospheric window. Observations of binary stars taken with the same instrumental configurations were reported by Monnier et al. (2004b) and Kraus & Schloerb (2004). We report here the results of the first phase of our program in which we have studied 56 evolved giants (Tables 1 & 2) including 35 Mira stars, 18 SR variables and 3 Irr variables<sup>1</sup> looking for asymmetry in their brightness profiles.

We report observations taken during six observing runs during May 2002 to May 2003. Observations were taken either with a standard H band filter ( $\lambda_o = 1.65 \mu\text{m}$ ,  $\Delta\lambda = 0.3 \mu\text{m}$ ) or with a narrow-band filter ( $\lambda_o = 1.64 \mu\text{m}$ ,  $\Delta\lambda = 0.1 \mu\text{m}$ ). Typically, five minutes of program star observations were followed by nearby calibrator observations under identical instrumental configurations. For the observations taken during March 2003 and May 2003 observing runs, we used ND filters for the bright targets since we had excellent optical throughput with newly coated primary mirrors and well optimized beam-train. On each star, we record 4 sets of data files each containing about 500 scans. A scan consists of changing the optical path difference between two beams by roughly  $75 \mu\text{m}$  in saw tooth form. We then take about 400 scans of shutter data for calibration. The shutter data sequence consists of allowing only one beam at a time (telescope A, B and then C) and at the end blocking all three beams. Each scan takes about 100 ms.

---

<sup>1</sup> $\delta$ 2 Lyr is classified in the Combined General Catalogue of Variable Stars (CGCVS; Samus et al. (2004)) with an uncertainty as a SR variable, and no period estimation is available in the literature. We consider this target as being an Irr variable for the purpose of this paper.

All targets were observed with a three-baseline interferometer configuration, forming a closed triangle. Earth rotation enables closure-phase measurements at slightly different projected baselines (and hence different closed triangles) when observations are made at different hour angles. We have adopted baseline bootstrapping (Mozurkewich & Armstrong 1992) at the IOTA whereby fringes are tracked on two short baselines, while science data are recorded on all three baselines simultaneously, enabling low visibility measurements on the third (long) baseline. Details of the detector camera and the fringe tracker algorithm used for this work are reported by Pedretti et al. (2004) and Pedretti et al. (2005) respectively.

IOTA’s maximum baseline of  $B=38$  m yields an angular resolution of  $\lambda/2B \simeq 4$  mas at  $1.65 \mu\text{m}$ . The present faint limit with the IONIC beam-combiner is  $H \simeq 7$  for the broad band filter and  $H \simeq 5$  for the three narrow band filters. For the difficult case of observing well resolved Mira stars with the H filter at or below 5% visibility level, the limiting magnitude is  $H \simeq 4$ . The limiting magnitude of the star tracker at IOTA, for these observations, was  $V \simeq 12$  for late-type stars. The angular resolution of our short south-east arm at IOTA is lower than that of the North-east arm, meaning that we could miss some asymmetry if it were predominantly parallel to the projected south-east baseline of the interferometer.

Pulsation periods for all Mira and SR variables (53 out of 56 program stars) are from Combined General Catalog of Variable Stars (CGCVS). Among these 53 program stars, 37 also have period estimations from American Association of Variable Star Observers (AAVSO) derived using a data window centered on JD 2452000 (Templeton, Mattei & Willson 2004) enabling us to validate the CGCVS periods. In addition, AAVSO has tentative or very tentative periods for three more SR stars. The CGCVS periods are consistent with available AAVSO periods for all but four of our program stars. Interestingly, the AAVSO periods for all four discrepant stars, namely X Cnc, BG Ser, UU Aur and W Ori, are roughly twice that of CGCVS periods although the AAVSO periods for two of them, namely UU Aur and W Ori, are either tentative or very tentative values. For completeness, one of the Irr variable, namely, TX PSc has a very tentative AAVSO period of 255.5 days.

### 3. Data Reduction

The recorded interferograms were reduced with an IDL code package developed by one of us (Ragland). Our single-mode integrated-optics beam-combiner chip (Berger et al. 2004) has 3 input beams ( $I_a, I_b, I_c$ ), and 6 output beams ( $I_i, i = 1 - 6$ ). Each input is split into 2 parts and coupled to the outputs as follows:  $(a, b) \leftrightarrow (1, 2)$ ;  $(a, c) \leftrightarrow (3, 4)$ ;  $(b, c) \leftrightarrow (5, 6)$ . The complimentary outputs ( $I_2, I_4$  &  $I_6$ ) have the same information as the normal outputs ( $I_1, I_3$  &  $I_5$ ) except for a  $\pi$  fringe intensity phase shift. Hence the normal and the

complimentary outputs could be combined in order to improve the signal to noise ratio of the measurements. The background subtracted outputs are combined two by two (with opposite signs) and normalized as follows, in order to remove scintillation noise which is common to both normal and complimentary outputs,

$$I_{ab} = \frac{I_1/\bar{I}_1 - I_2/\bar{I}_2}{2}, \quad (1)$$

and correspondingly for the other outputs. Here  $\bar{I}$  denotes the mean over the entire scan.

The power spectra of the resultant three outputs  $I_{ab}$ ,  $I_{bc}$  and  $I_{ac}$  are computed and the fringe power for each of these three outputs is estimated by integrating the power (P) under the fringe profile after background power subtraction (Baldwin et al. 1996). The fringe power is proportional to the visibility-squared ( $V^2$ ). The target  $V_{target}^2$  is calibrated by measuring the fringe power for a nearby calibrator of known  $V_{calib}^2$  under the same instrumental configuration and by taking the ratio. i.e.

$$V_{target}^2 = V_{calib}^2 \left( \frac{P_{target}}{P_{calib}} \right) \quad (2)$$

The closure phase is the sum of the fringe phases simultaneously observed on three baselines forming a closed triangle and is insensitive to phase errors induced by the turbulent atmosphere or optics (Jennison 1958). If the phase errors introduced into the three beams are  $\delta_a$ ,  $\delta_b$  and  $\delta_c$ , then the observed fringe phase between baselines a and b can be written as

$$\phi_{ab} = \psi_{ab} + \delta_b - \delta_a \quad (3)$$

Here  $\psi_{ab}$  is the true object fringe phase between baselines a and b.

The observed closure phase  $\Phi_{cl}$  is equal to the true object closure phase,  $\psi_{ab} + \psi_{bc} + \psi_{ca}$ , to within the measurement noise, as follows:

$$\Phi_{cl} = \phi_{ab} + \phi_{bc} + \phi_{ca} + \text{noise} \quad (4)$$

$$= \psi_{ab} + \delta_b - \delta_a + \psi_{bc} + \delta_c - \delta_b + \psi_{ca} + \delta_a - \delta_c + \text{noise} \quad (5)$$

$$= \psi_{ab} + \psi_{bc} + \psi_{ca} + \text{noise} \quad (6)$$

We estimate closure phase as the phase of the bispectrum (Weigelt 1977) of simultaneous fringes obtained with the three baselines. The instrumental closure phase is estimated using a nearby calibrator and subtracted from the raw closure phase of the target to give a calibrated target closure phase.

Typical one-sigma formal errors in our uncalibrated closure phase and  $V^2$  measurements are  $\sim 0.2^\circ$  and  $\sim 2\%$  respectively. The formal errors are estimated from the scatters of the 500 fringe scans. In the case of  $V^2$  errors, the error due to background power subtraction is also incorporated into the formal error. The calibration process adds up additional errors and the measurement error is estimated as the square-root of the sum of the squares of the formal and calibration errors. The one-sigma measurement error is reported in Tables 1 & 2. We estimate calibration errors by observing calibrators under same observing condition and calibrating one calibrator with the other after accounting for the finite sizes of both calibrators. The estimated one-sigma calibration error is 5% for the  $V^2$  measurements and  $0.5^\circ$  for closure phase measurements. There could be unaccounted systematic errors in our measurements. For the purpose of this article, we adopt a systematic error of  $2^\circ$  for our closure phase measurements. The total error is estimated as the square-root of the sum of the squares of the formal, calibration and systematic errors. If the measured closure phase is less than twice the total error in the measurement then we call it essentially a non-detection of asymmetry. However, if it is larger, we call it positive detection. Further discussion on our visibility and closure phase measurements could be found in Ragland et al. (2004).

#### 4. Results

Targets with centro-symmetry should give a closure phase of either zero or  $\pm 180^\circ$  depending on how many baselines are beyond the 1st, 2nd, etc nulls. The majority of our targets show zero closure phase. However, 14 of the 56 have non-zero closure phase. Of these, 12 are Mira stars, and 4 are SR/Irr variable carbon stars. Among the 12 Mira stars, all but  $\chi$  Cyg are oxygen-rich Mira stars;  $\chi$  Cyg is classified as an S star. The frequency of asymmetry from our studies is 34% in Mira stars, 17% in SR variables, 33% in Irr variables and thus 29% in our entire sample of AGB stars. In terms of chemistry, the frequency of asymmetry is 33% in carbon stars and 27% in oxygen-rich stars.

Table 1 gives the measured closure phases along with observational and target information for these 14 targets that show measurable asymmetry from our observations. We have included in this table one observation each for R Cnc, R LMi & V Hya in which no asymmetry is detected since we use these observations for size estimation. All targets (except R Aur,  $\chi$  Cyg & UU Aur) have follow up measurements taken with all three narrow band filters to characterize the observed asymmetry. These results will be presented elsewhere. The  $V^2$  data for these targets are fitted with uniform disk (UD) models (figure 1) and the measured angular sizes are also given in Table 1. Table 2 lists targets for which we have not detected asymmetry from our survey. The calibrators used for our observations are also

listed in these tables. The angular sizes for most of the calibrators are taken from Wesselink, Paranya & de Vorkin (1972). Typically, we use calibrators with angular sizes less than 3 mas for our measurements. However, during the early part of the survey, we had to use larger calibrators because of low throughput of the instrument. We adopted the measured sizes from interferometric technique for  $\alpha$  Vul and  $\gamma$  Sge (Hutter et al. 1989), and from lunar occultation measurements for UU Aur (Bohme 1978). We estimated the angular size of 7 Peg from V and K magnitudes (van Belle 1999).



Table 1. Derived closure phase and UD diameters in the H band for targets with detected asymmetry.

Target	Date UT	Calibrator	Calib. diam. (mas)	CGCVS Period (days)	AAVSO Period (days)	Phase	Sp. Type	$B_{max}$ (cm)	$\theta_{UD}$ (mas)	$\phi_{cp}^5$ (deg)
<b>(a) Mira Stars:</b>										
IK Tau <sup>3</sup>	19Jan03	63 Ari	2.6	470		0.4	M6e-M10e	3282.1	24.72±0.23	117.3±1.0
	29Jan03							3282.3		162.4±17.4
	30Jan03							3309.1		152.8±2.9
								3287.0		144.4±3.2
R Aur <sup>3</sup>	19Jan03	HD 31312	2.6	457.5	452.5	0.4	M6.5e-M9.5e	3461.5	10.01±0.20	-7.0±0.5
	25Jan03							3416.9		-6.6±0.6
	28Jan03							3487.0		-6.7±0.6
U Ori <sup>3</sup>	28Jan03	40 Ori	2.2	368.3	372.3	0.1	M6e-M9.5e	3461.6	11.31±0.41	-8.6±0.6
S CMi	08Mar03	27 Mon	2.4	332.9	329.6	0.4	M7e	3520.4	7.06±0.08	6.0±0.6
R Cnc <sup>3</sup>	23Jan03	$\omega$ Hya	2.5	361.6	362.3	0.3	M6e-M9e	3354.7	12.65±0.35	6.7±0.6
								3131.8		-1.0±0.7 <sup>1</sup>
	28Jan03							3424.7		9.6±0.7
R LMi <sup>2,3</sup>	07Mar03	$\omega$ Hya	2.5	372.2	375.4	0.5	M7e	2916.8	13.16±0.21	2.6±0.5 <sup>1</sup>
	09Mar03							3825.4		-5.6±1.2
	12Mar03							3582.7		-31.5±0.8
S CrB	07Mar03	HR 5464	2.7	360.3	365	0.5	M7e	2914.3	8.81±0.16	5.5±0.5
RU Her <sup>2</sup>	10Mar03	51 Her	2.5	484.8	494.1	0.1	M6e-M9	3823.6	8.00±0.20	-7.2±0.7
	11Mar03							3539.3		-6.6±0.6
	13Mar03							3530.0		-11.0±0.7

Table 1—Continued

Target	Date UT	Calibrator	Calib. diam. (mas)	CGCVS Period (days)	AAVSO Period (days)	Phase	Sp. Type	$B_{max}$ (cm)	$\theta_{UD}$ (mas)	$\phi_{cp}$ <sup>5</sup> (deg)
U Her <sup>3</sup>	28Jun02	$\kappa$ Ser	6.6	406.1	406.5	0.0	M6.5e-M9.5e	3657.9	9.69±0.37	20.9±1.6
R Aql <sup>3</sup>	27Jun02	$\gamma$ Sge	6.9	284.2	272.9	0.7	M5e-M9e	3385.9	12.72±0.20	-26.6±0.8
$\chi$ Cyg <sup>3</sup>	29May02	$\alpha$ Vul	5.1	408.1	404.8	0.2	S6,2e-S10,4e	2121.9	22.59±0.52	168.7±1.4
R Aqr <sup>3</sup>	30Oct02	$\iota$ Cet	4.7	387.0	386.1	0.3	M5e-M8.5e+pec	2614.3	19.07±0.08	-11.0±0.9
<b>(b) Semi-regular Variables:</b>										
UU Aur <sup>3</sup>	30Jan03	HD 61603	2.9	234	(457.5)		C5,3-C7,4	3554.4	10.88±0.18	-15.5±0.6
V Hya <sup>2</sup>	10Mar03 11Mar03	$\alpha$ Crt	2.9	530.7		0.1	C6,3e-C7,5e	2655.2 2666.6	21.23±2.77 <sup>4</sup>	17.4±0.7 0.4±0.6 <sup>1</sup>
Y CVn <sup>3</sup>	28Jan03	HR 5464	2.7	157			C5,4J	3487.7	14.05±0.73	-26.9±1.8
<b>(c) Irregular Variables:</b>										
TX PSc <sup>3</sup>	29Oct02 30Oct02	$\iota$ Cet	4.7		(255.5)		CII...	3336.5 3234.3	9.89±0.17	-4.6±0.7 -1.5±0.7 <sup>1</sup>

<sup>1</sup>This observation doesn't show asymmetry.<sup>2</sup>Observed with the narrow band filter at 1.64 $\mu$ m.<sup>3</sup>At least one of the baseline resolved this target to the level of below 5% in V<sup>2</sup>.

<sup>4</sup>UD model failed to fit the data. The derived value probably gives the diameter of the dust shell rather than diameter of central star.

<sup>5</sup>The uncertainties indicates random errors only (see text).

Six of our targets with detected asymmetry, namely, U Ori, R Cnc, R LMi, S CrB, R Aql, R Aqr have earlier H band size measurements (Millan-Gabet et al. 2005) taken within  $\pm 0.2$  pulsation phase with respect to the pulsation phase of our measurements for these stars. We have plotted our size measurements against the measurements by these authors for these six targets in Figure 2. The scatter in this figure is comparable to the scatter among measurements of a given star at multiple epochs in a single program, and thus probably either signifies actual size variation at the source or that the interpretation of the observations (UD) is too simple. Several targets have earlier K band angular size measurements (van Belle et al. (1996); van Belle, Thompson & Creeck-Eakman (2002); Millan-Gabet et al. (2005); Mennesson et al. (2002); Dyck, van Belle & Benson (1996)).

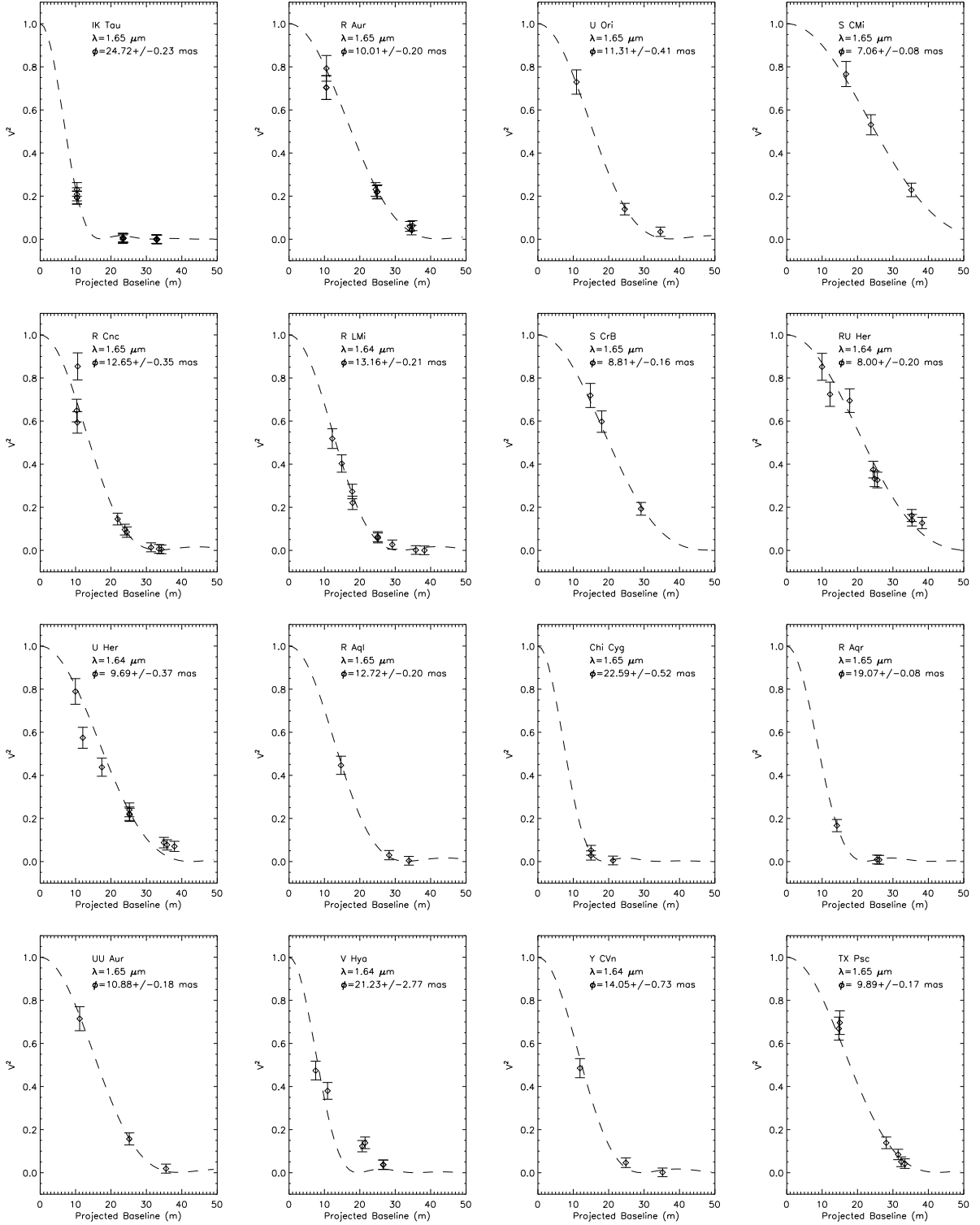


Fig. 1.— Visibility-data fitted with an UD model for the targets with positive asymmetry detection from our observations. UD models fits the data very well except for V Hya. In the case of V Hya, the derived size is possibly the size of the dust shell rather than that of the central star.

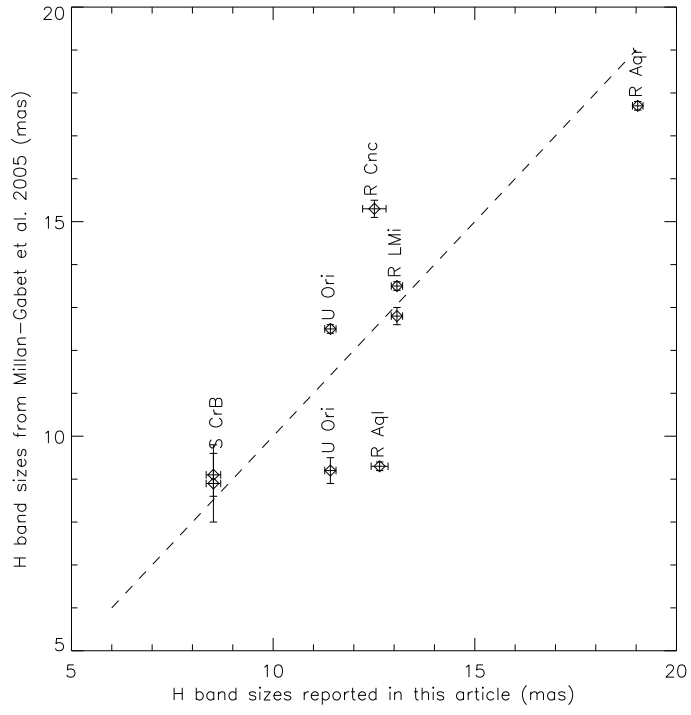


Fig. 2.— Shows the comparison of sizes reported in this article with those reported in the literature.

Table 2. Closure phase measurements for targets with no detectable asymmetries

Target	Date UT	Calib.	CGCVS Period (days)	AAVSO Period	Phase	Sp. Ty. (cm)	$B_{max}$ (mas)	$\theta_{UD}$ (deg)	$\phi_{cp}^{15}$
<b>(a) Mira Stars:</b>									
U Per	30Oct02	51 And	320.3	318.7	0.5	M6e	3607.2	5.84 <sup>2</sup>	1.4±1.1
R Tri	29Jan03	24 Per	266.9	264.8	0.9	M4IIIe	3548.7	4.46 <sup>3</sup>	2.8±0.5
RT Eri	31Jan03	HR 1543	370.8	376.5	0.9	M:e	2527.9	6.3 <sup>4</sup>	1.0±0.6
R Lep <sup>1</sup>	31Jan03	HR 1543	427.1	437.8	0.8	CIIe...	2904.8	11.50 <sup>5</sup>	-3.9±0.6
RU Aur	29Jan03	51 Ori	466.5	464.3	0.7	M8	3553.5	3.7 <sup>4</sup>	-0.9±0.6
X Aur	29Oct02	$\nu$ Aur	163.8	166.1	0.2	K2	3664.0	1.8 <sup>4</sup>	2.5±1.1
	23Jan03	HD 31312			0.2		3378.4		-0.2±0.6
	25Jan03				0.2		3429.5		-0.9±0.6
	28Jan03				0.2		3507.5		-2.1±0.6
V Mon	29Jan03		340.5	332.7		M6e	2771.1	5.6 <sup>4</sup>	2.6±0.6
W Cnc	28Jan03	$\omega$ Hya	393.2	391.8	0.3	M7e	3415.2	4.7 <sup>4</sup>	-0.7±0.6
X Hya	30Jan03	28 Hya	301.1	301.2	0.6	M7e	2451.7	5.0 <sup>4</sup>	-0.2±0.6
R LMi	28Jan03	HR 5464	372.2	375.4	0.3	M7e	3530.8	13.2 <sup>2</sup>	-2.6±0.7
V Boo	29May02	$\rho$ Boo	258.0	261.1	0.6	M6e	2100.6	5.2 <sup>4</sup>	-0.7±0.7
	28Jan03	HR 5464			0.6		3448.6		0.2±0.6
S CrB	29May02	52 Boo	360.3	365	0.7	M7e	2121.3	9.1 <sup>2</sup>	0.3±0.8
	28Jan03	HR 5464			0.4		3509.1	8.9 <sup>2</sup>	1.5±0.6
S Ser	28Jun02	$\kappa$ Ser	371.8	373.7	0.9	M5e	3557.1	5.35 <sup>6</sup>	-1.3±1.5
BG Ser	29Jun02	$\kappa$ Ser	143	386.1	0.7	M6me...	3042.7	6.71 <sup>6</sup>	0.1±0.9

Table 2—Continued

Target	Date UT	Calib.	CGCVS Period (days)	AAVSO Period	Phase	Sp. Ty. (cm)	$B_{max}$ (mas)	$\theta_{UD}$ (deg)	$\phi_{cp}^{15}$
	30Jan03	110 Vir			0.3		3328.4		0.7±0.7
							3305.8		-0.2±0.7
R Ser	27May02	$\kappa$ Ser	356.4	355.6	0.4	M7IIIe	2089.8	7.6 <sup>2</sup>	0.0±1.0
	28May02	$\kappa$ Ser			0.4		2052.9		0.4±0.8
V CrB	30Jan03	HR 5464	357.6	361.3	0.9	N...	3271.8	7.26 <sup>5</sup>	-1.5±0.6
RU Her	25May02	HR 5947	484.8	494.1	0.5	M7e...	2116.5	8.71 <sup>6</sup>	1.3±0.9
RT Oph	28Jun02	$\beta$ Oph	426.3	424.8	0.0	M7	3500.1	6.52 <sup>6</sup>	-1.0±1.0
X Oph	26May02	$\gamma$ Aql	328.9	341.1	0.4	K1III+...	1968.1	12.97 <sup>3</sup>	-0.6±0.8
R Aql	26May02	$\gamma$ Aql	284.2	272.9	0.5	M7IIIe	1944.2	9.3 <sup>2</sup>	-1.1±0.8
W Aql	28May02	$\gamma$ Aql	490.4	480.8	0.1	S:...	1650.0	11.08 <sup>5</sup>	1.2±1.0
RT Aql	24Jun02	$\gamma$ Aql	327.1	325.7	0.0	M7e	3488.8	7.24 <sup>6</sup>	1.9±0.8
BG Cyg	29Jun02	$\gamma$ Sge	228	285.4	0.1	M7e	3793.5	4.14 <sup>6</sup>	-1.8±1.0
RR Aql	28May02	$\gamma$ Aql	394.8	398.7	1.0	M7e	1795.9	10.73 <sup>6</sup>	0.2±1.0
U Cyg	28Jun02	$\beta$ Oph	463.2	469	0.0	R...	3732.1	7.05 <sup>5</sup>	-3.5±1.4
V1426 Cyg	30Oct02	$\rho$ Cyg	470	481.2	0.9	C	3816.0	10.8 <sup>7</sup>	-0.8±0.9
R Peg	31Oct02	7 Psc	378.1	378.2	0.8	M7e	3579.7	7.0 <sup>2</sup>	-1.9±1.2
<b>(b) Semi-regular Variables:</b>									
$\rho$ Per	21Nov02	24 Per	50			M4II		15.53 <sup>8</sup>	1.3±3.5
W Ori	31Oct02	40 Ori	212	(446)		CII...	3394.3	9.7 <sup>7</sup>	5.2±1.8
CE Tau	30Oct02	HD 33554	165			M2Iab:	3717.4	9.1 <sup>9</sup>	-4.1±1.2



Table 2—Continued

Target	Date UT	Calib.	CGCVS Period (days)	AAVSO Period	Phase	Sp. Ty. (cm)	$B_{max}$ (mas)	$\theta_{UD}$ (deg)	$\phi_{cp}$ <sup>15</sup>
X Cnc	19Jan03	$\omega$ Hya	195	379.6	0.3	CII...	3527.5	7.62 <sup>10</sup>	1.8±0.6
	25Jan03				0.3		3473.1		-0.4±0.6
	28Jan03				0.3		3410.5		2.1±0.6
T Cnc	23Jan03	$\omega$ Hya	428	499.5		N...	3447.1	6.6 <sup>11</sup>	-2.0±0.6
	28Jan03						3409.6		0.3±0.6
U Hya	25Jan03	$\alpha$ Crt	450			CII...	2902.0	10.8 <sup>4</sup>	-2.4±0.7
	30Jan03	HR 5464					2489.6		-2.8±0.6
V Hya	23Jan03	$\alpha$ Crt	530.7		1.0	C...	2640.1	13.0 <sup>4</sup>	2.1±0.6
Y CVn	29May02	HR 4690	157			CIab:...	2022.7	11.6 <sup>7</sup>	-3.6±1.0
RT Vir	28May02	$\nu$ Boo	155			M8III	1902.3	12.38 <sup>12</sup>	0.7±0.7
SW Vir	28May02	$\nu$ Boo	150	155.4		M7III	1818.9	16.24 <sup>12</sup>	2.8±0.9
RX Boo <sup>1</sup>	23May02	$\rho$ Boo	340			M7.5	2112.2	17.48 <sup>12</sup>	-3.9±1.0
ST Her	23May02	HR 5763	148			M6s	1945.5	9.3 <sup>13</sup>	-0.1±1.0
X Her	25May02		95			M		12.1 <sup>13</sup>	
g Her <sup>1</sup>	29May02	52 Boo	89.2			M6III	2063.0	12.67 <sup>12</sup>	-2.5±1.0
R Lyr <sup>1</sup>	25May02	HR 6695	46			M5III	2056.4	13.3 <sup>13</sup>	0.3±0.9
V Aql	28Jun02	$\beta$ Oph	353	377.1		CII...	2870.1	10.1 <sup>7</sup>	-0.8±1.0
EU Del	26May02	$\gamma$ Sge	59.7		0.7	M6III	2063.7	9.8 <sup>9</sup>	-0.8±0.8
<b><u>(c) Irregular Variables:</u></b>									
Del2 Lyr	25May02	HR 6695				M4II	2099.3	10.32 <sup>14</sup>	-0.6±0.9



<sup>12</sup>Menesson et al. (2002)

<sup>13</sup>Dyck et al. (1996)

<sup>14</sup>Sudol et al. (2002)

<sup>15</sup>The uncertainties indicates random errors only (see text).

Out of 56 AGB stars, 16 are well resolved (i.e. at least one baseline gives a  $V^2$  measurement less than 5% of the point source value) from our observations. Among these 16 targets, 12 of them show asymmetry from our observations. Thus, if we consider only well resolved targets, 75% of AGB stars show asymmetry. Targets from our measurements that are well resolved are marked in Tables 1 & 2 (see the footnote). Interestingly, all well resolved targets that don't show asymmetry (except R Lep), namely, g Her, R Lyr & RX Boo are SR variables; R Lep is a carbon Mira. Thus, if we consider only well-resolved oxygen rich Mira stars then our asymmetry detection is 100% and in the case of SR variables the success rate is 40%. The well-resolved Mira variable R LMi did not show asymmetry from our January 2003 observations. However, we detected asymmetry in this target during March 2003 observations. Similarly, the well-resolved Irr variable TX Psc did not show asymmetry from our June 2002 measurements. However, we detected asymmetry in TX Psc from our follow-up observations taken in October 2002.

At least five targets with detected asymmetry, namely, S CrB, RU Her, R Aql, V Hya and Y CVn have earlier measurements taken with relatively shorter baselines and we did not detect asymmetry from these measurements.

In order to understand the role of angular resolution on the asymmetry detection, we derived the number of pixel elements ( $N_{pix}$ ) in an imaging sense, defined as the angular diameter divided by the angular resolution ( $\lambda/2B_{max}$ ) for all targets. Here  $B_{max}$  is the maximum baseline of our observations listed in Tables 1 & 2 for all our targets. We plotted our measured closure phase values against number of pixel elements in Figure (3). This figure clearly shows that the positive closure phase cases are those that have pixel elements close to or greater than unity, meaning they are well resolved. This suggests that the detected asymmetry features are probably on the surface of the stellar disk or visible only in projection against the stellar disk (such as might be the case for patchy dust opacity at 1.5 to 2.5 stellar radii).

## 5. Simple Models

We have assumed a 2-component brightness distribution model in order to find the simplest possible implications of the measured closure phase signal. This model consists of a uniform-disk star with an intensity distribution  $\tilde{I}_p(\vec{r})$  and an unresolved secondary component (bright spot, companion or dust clump) with an intensity distribution  $\tilde{I}_s(\vec{r} - \vec{\delta r})$ , where  $\vec{\delta r}$  is the separation vector between the optical centers of the components. The total intensity is  $I = \tilde{I}_p(\vec{r}) + \tilde{I}_s(\vec{r} - \vec{\delta r})$ . The complex visibility is the Fourier transform of the brightness distribution. Thus, the complex visibility of this composite object could be written using

the shift theorem for Fourier transforms as

$$\hat{V}(\vec{g}) = \hat{V}^p(\vec{g}) + \hat{V}^s(\vec{g}) e^{ik\vec{g}\cdot\vec{\delta r}} \quad (7)$$

where  $k = 2\pi/\lambda$ ,  $\lambda$  is the wavelength of observation and  $\vec{g}$  is the baseline vector  $\vec{B}$ .

The complex visibility for the baseline  $\vec{B}_{AB}$  could be written as

$$\hat{V}_{AB} = V_{AB}^p e^{i\phi_{AB}^p} + V_{AB}^s e^{i\phi_{AB}^s} e^{ik\vec{B}_{AB}\cdot\vec{\delta r}} \quad (8)$$

The visibility phase for the baseline  $B_{AB}$  is

$$\phi_{AB} = \arctan \left[ \frac{Im \hat{V}_{AB}}{Re \hat{V}_{AB}} \right] \quad (9)$$

$$= \arctan \left[ \frac{V_{AB}^p \sin(\phi_{AB}^p) + V_{AB}^s \sin(\phi_{AB}^s + k\vec{B}_{AB}\cdot\vec{\delta r})}{V_{AB}^p \cos(\phi_{AB}^p) + V_{AB}^s \cos(\phi_{AB}^s + k\vec{B}_{AB}\cdot\vec{\delta r})} \right] \quad (10)$$

$$= \arctan \left[ \frac{V_{AB}^p \sin(\phi_{AB}^p) + V_{AB}^s \sin(\phi_{AB}^s) \cos(k\vec{B}_{AB}\cdot\vec{\delta r}) + V_{AB}^s \cos(\phi_{AB}^s) \sin(k\vec{B}_{AB}\cdot\vec{\delta r})}{V_{AB}^p \cos(\phi_{AB}^p) + V_{AB}^s \cos(\phi_{AB}^s) \cos(k\vec{B}_{AB}\cdot\vec{\delta r}) - V_{AB}^s \sin(\phi_{AB}^s) \sin(k\vec{B}_{AB}\cdot\vec{\delta r})} \right] \quad (11)$$

The individual components of the brightness distributions are assumed to be circularly symmetric. Hence,  $\sin(\phi_{AB}^p) = \sin(\phi_{AB}^s) = 0$ , but  $\cos(\phi_{AB}^p)$  and  $\cos(\phi_{AB}^s)$  can be +1 or -1, depending on details of the case. Thus,

$$\phi_{AB} = \arctan \left[ \frac{V_{AB}^s \cos(\phi_{AB}^s) \sin(k\vec{B}_{AB}\cdot\vec{\delta r})}{V_{AB}^p \cos(\phi_{AB}^p) + V_{AB}^s \cos(\phi_{AB}^s) \cos(k\vec{B}_{AB}\cdot\vec{\delta r})} \right] \quad (12)$$

### Unresolved Secondary component:

For an unresolved (i.e. a point source)  $\phi_{AB}^s = 0$ . Thus,

$$\phi_{AB} = \arctan \left[ \frac{V_{AB}^s \sin(k\vec{B}_{AB}\cdot\vec{\delta r})}{V_{AB}^p \cos(\phi_{AB}^p) + V_{AB}^s \cos(k\vec{B}_{AB}\cdot\vec{\delta r})} \right] \quad (13)$$

For a uniform-disk star,

$$\hat{V}_{AB}^p = \left[ \frac{2J_1(\pi N_{pix}^{AB}/2)}{\pi N_{pix}^{AB}/2} \right] I_p, \quad (14)$$

and

$$V_{AB}^p \cos(\phi_{AB}^p) = \left[ \frac{2J_1(\pi N_{pix}^{AB}/2)}{\pi N_{pix}^{AB}/2} \right] I_p, \quad (15)$$

For an unresolved secondary component,

$$V_{AB}^s = I_s, \quad (16)$$

where  $I_p$  and  $I_s$  are the normalized star and secondary component intensities (i.e.  $I_p + I_s = 1$ ), and

$$N_{pix}^{AB} = \frac{\theta_{UD}}{(\lambda/2B_{AB})} \quad (17)$$

Combining eqn (13), (15) and (16), we get

$$\phi_{AB} = \arctan \left[ \frac{I_s \sin(k\vec{B}_{AB} \cdot \vec{\delta r})}{I_p \left( \frac{2J_1(\pi N_{pix}^{AB}/2)}{\pi N_{pix}^{AB}/2} \right) + I_s \cos(k\vec{B}_{AB} \cdot \vec{\delta r})} \right] \quad (18)$$

### Resolved Secondary component:

For a resolved Gaussian secondary component (such as dust clump)  $\phi_{AB}^s = 0$ , and

$$V_{AB}^s = \left[ \exp(-(\pi\beta N_{pix}^{AB}/2\alpha)^2) \right] I_s \quad (19)$$

where,  $\alpha = 2\sqrt{\ln(2)}$  and  $\beta$  is the ratio of the size of the primary component to the secondary.

Thus,

$$\phi_{AB} = \arctan \left[ \frac{I_s \exp(-(\pi\beta N_{pix}^{AB}/2\alpha)^2) \sin(k\vec{B}_{AB} \cdot \vec{\delta r})}{I_p \left( \frac{2J_1(\pi N_{pix}^{AB}/2)}{\pi N_{pix}^{AB}/2} \right) + I_s \exp(-(\pi\beta N_{pix}^{AB}/2\alpha)^2) \cos(k\vec{B}_{AB} \cdot \vec{\delta r})} \right] \quad (20)$$

For a resolved uniform-disk secondary component (such as stellar companion)  $\phi_{AB}^s = 0$  or  $\pm\pi$ , and

$$\hat{V}_{AB}^s = \left[ \frac{2J_1(\pi\beta N_{pix}^{AB}/2)}{\pi\beta N_{pix}^{AB}/2} \right] I_s, \quad (21)$$

and

$$V_{AB}^s \cos(\phi_{AB}^s) = \left[ \frac{2J_1(\pi\beta N_{pix}^{AB}/2)}{\pi\beta N_{pix}^{AB}/2} \right] I_s, \quad (22)$$

Now,

$$\phi_{AB} = \arctan \left[ \frac{I_s \left( \frac{2J_1(\pi\beta N_{pix}^{AB}/2)}{\pi\beta N_{pix}^{AB}/2} \right) \sin(k\vec{B}_{AB} \cdot \vec{\delta r})}{I_p \left( \frac{2J_1(\pi N_{pix}^{AB}/2)}{\pi N_{pix}^{AB}/2} \right) + I_s \left( \frac{2J_1(\pi\beta N_{pix}^{AB}/2)}{\pi\beta N_{pix}^{AB}/2} \right) \cos(k\vec{B}_{AB} \cdot \vec{\delta r})} \right] \quad (23)$$

Using eqn (4), (18), (20) and (23), we generate closure phase models for the IOTA configuration A35B15C00 (i.e.  $B_{CA} = 35$  m;  $B_{BC} = 15$  m) which are shown with our data in Figure 3. We explored the parametric space with four cases, namely (1) surface-unresolved spot, (2) surface-unresolved companion, (3) surface-resolved companion and (4) surface-resolved Gaussian dust clump. The values assumed for various parameters of these models are primarily for the purpose of illustration. More thorough treatment of the physical parameters chosen in the models will be presented in the forthcoming article. We have shown two models for each of the four cases (totally eight models) in Figure 3. The two models differ only in the position angle of the secondary feature - one assumes the secondary feature at the position angle of  $21.8^\circ$  and the other at the position angle of  $201.8^\circ$  (i.e. a  $180^\circ$  rotation). The reason for choosing this axis (along the direction of the largest baseline of the IOTA array) is that the closure-phase signal is approximately maximum when the secondary feature is assumed along this axis. The brightness distribution of the primary component is assumed to be an uniformly illuminated disk. The flux of the secondary component is assumed to be 3% of the total flux for surface-unresolved secondary cases and 30% for surface-resolved secondary component cases; the reason for choosing these flux values for the companion is that the corresponding models compare well with our closure phase measurements. The spot models (case 1) assume a surface-unresolved bright spot at the edge of the stellar disc ( $\delta r = \theta_{UD}/2$ ). The surface-unresolved binary models (case 2) assume a surface-unresolved companion or dust clump at 5 stellar radii ( $\delta r = 2.5 \theta_{UD}$ ). The surface-resolved binary models (case 3) assume companion with  $\beta = 0.99$  (UD angular size of the secondary component is 99% of the primary) at 5 stellar radii ( $\delta r = 2.5 \theta_{UD}$ ). If companion stars provide enough light to produce detectable asymmetry near maximum light, then they should also produce a wider, flattened, minima in the light curves (Merrill 1956). While at least two of the stars are known binaries and relatively mild symbiotic systems (R Aqr and o Ceti) none of the stars show a filled-in minimum on the AAVSO light curves. The dust models (case 4) assume a Gaussian shaped dust clump ( $\beta = 1$ ; same equivalent size as the primary component) at 5 stellar radii ( $\delta r = 2.5 \theta_{UD}$ ). As can be seen in Figure 3, the unresolved spot models compare well with the observed data and the unresolved companion models are not as good as the unresolved spot models in explaining the observed closure phase data. The resolved secondary feature models (case 3 & 4) show that the secondary components have to be significantly brighter (may be physically unreasonable) in order to produce detectable closure phase signals and even so, the fits at low  $N_{pix}$  are poor.

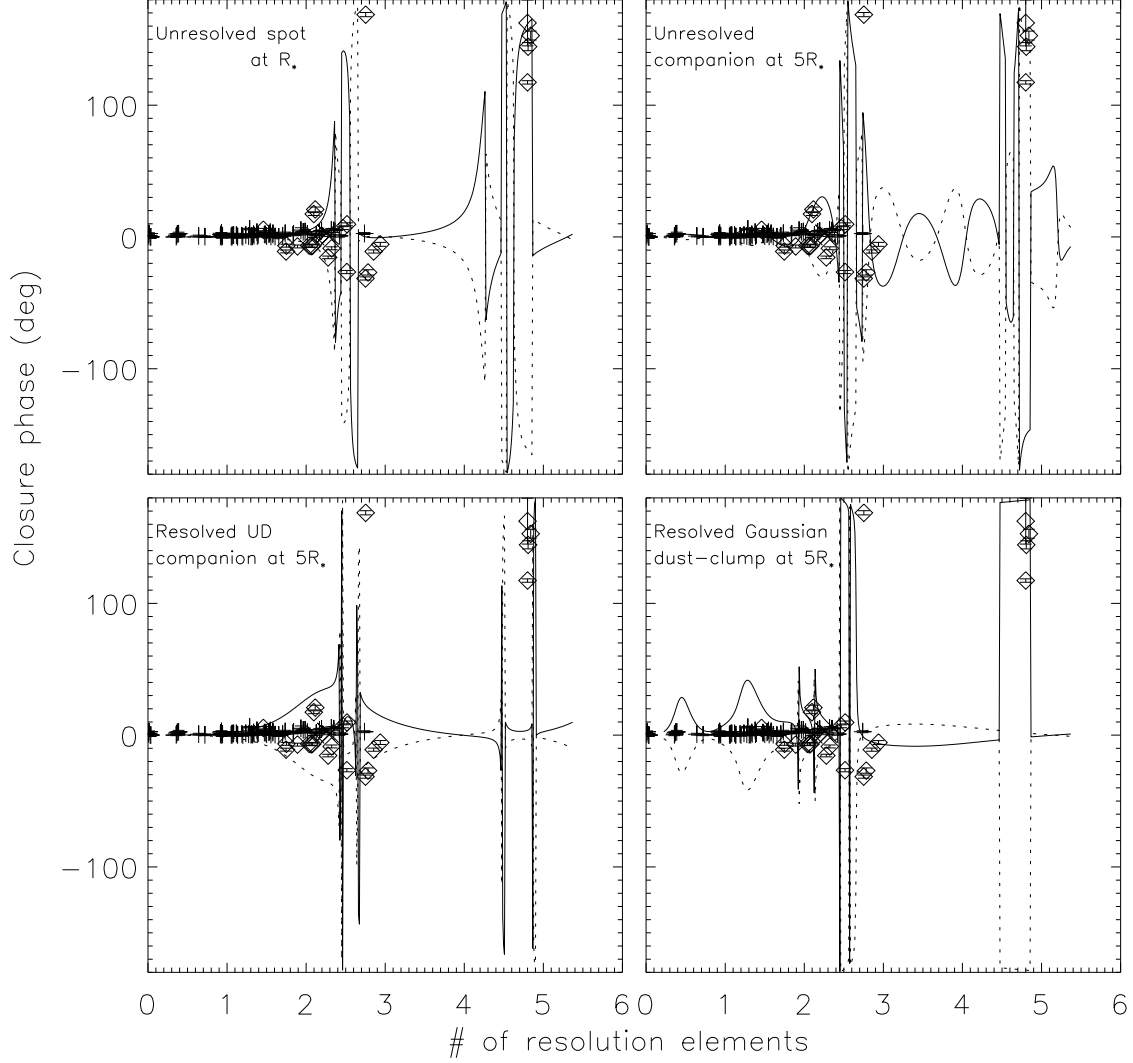


Fig. 3.— Measured closure phases are plotted against number of pixel elements (see the text). Targets with positive asymmetry detection are shown as diamond symbols and non-detection measurements are shown as plus symbols. Targets that are well resolved frequently show large closure phase. The solid lines refer models where the secondary feature is assumed at the position angle of  $21.8^\circ$  (along the direction of the largest baseline of the IOTA array) and the dotted lines refer to models where the secondary feature is assumed at the position angle of  $201.8^\circ$  ( $21.8^\circ + 180^\circ$ ). The flux of the unresolved secondary components are assumed to be 3% and that of the resolved secondary component is assumed to be 30%. Top left: Unresolved spot at the edge of the stellar disc ( $\delta r = \theta_{UD}/2$ ); Top right: Unresolved companion at 5 stellar radii ( $\delta r = 2.5 \theta_{UD}$ ); Bottom left: Resolved UD companion at 5 stellar radii ( $\delta r = 2.5 \theta_{UD}$ ); The diameter of the secondary is assumed to be 99% of the diameter of the primary; Bottom right: Resolved Gaussian dust clump at 5 stellar radii ( $\delta r = 2.5 \theta_{UD}$ ); The equivalent size of the secondary is assumed to be same as that of the primary.



## 6. Discussion

The significance of the present results (i.e., that 1/3 are asymmetric and 2/3 are not) depends on what causes the asymmetry, and that is not yet known. As noted in the introduction, although planetary nebulae are predominantly bipolar, a large fraction (possibly even all) of proto-PN are axisymmetric inside an apparently spherical AGB wind remnant, suggesting that the PN asymmetry has arisen only after or as the star left the AGB. Asymmetries have been reported before for Miras, but these are mostly for isolated examples, or for maser emission that is very sensitive to the local conditions and thus will tend to exaggerate any physical departure from spherically symmetric flow. The present results, referring to intensity near the stellar flux maximum, are much less sensitive to small variations in the conditions. It's worth mentioning here that the non-detections don't preclude asymmetries. It could be that they are just not resolved or the asymmetries are too small.

The SiO maser emission also arises well above the photosphere (e.g. Humphreys et al 2002; Cotton et al. (2004)); in fact, there is, to our knowledge, no report yet of asymmetry that can be assigned unambiguously to the stellar surface. With multiple narrow-band measurements at carefully selected wavelengths, Perrin et al (2004) have shown that it is possible to disentangle photospheric and shell contributions. The results reported here suggest that we will also be able to sort out some shape information in the next generation of observations as well as separate the photospheric contribution from the circumstellar one.

There is a considerable literature concerning the non-circular and non-spherical symmetry common among planetary nebulae; see, for example, the proceedings of *Asymmetric Planetary Nebulae III* (2004, ASP Conf. Ser. 313). Mechanisms may be roughly divided into deep and superficial. Deep mechanisms include internal convective structure with large convection cells (proposed by Schwarzschild (1975) on the basis of simple scaling arguments), non-radial pulsation, and/or rotation.

These stars have massive envelopes and large radii; no reasonable reservoir of angular momentum other than incorporation of a relatively massive ( $> 0.1 M_{\odot}$ ) companion will provide sufficient angular momentum for rotational asymmetry or the usual non-radial-pulsation associated with rotation. Large convective cells might stimulate non-radial modes in the absence of significant rotation, or might lead to modulations in the surface brightness from rising or falling elements. Evolutionary models show a radiative layer above the convective layer in these stars (Ostlie & Cox 1986) and the scale heights at the photosphere are only a percent or so of  $R_{*}$ ; these facts suggest that convective modulation will be on a smaller scale and with less contrast than is needed to explain these observations, but more detailed modeling should be done before the possibility of convection-based modulation is ruled out.

Superficial or atmospheric mechanisms include magnetic structures (e.g. Soker & Zoabi 2002; Blackman et al. 2001), discrete dust cloud formation as for R CrB stars, and interaction of a planet or companion with the stellar wind (Struck, Cohanin & Willson 2004; Mastrodemos & Morris 1998, 1999). The conclusion that perhaps all of the Miras show some asymmetry while only about half of the non-Miras do may be understood in a couple of ways. Miras comprise a well-defined subset of long period variables, namely those with large visual amplitudes, relatively regular variation, cool effective temperatures, and moderate progenitor masses. SR classes differ in visual amplitude (SRa), degree of irregular variation (SRb), warmer effective temperature (SRd), and higher progenitor mass (SRc). Within each of these classes there are further probable subclasses. Our current understanding is that the high visual amplitude is partly the result of variable atmospheric opacity (Reid & Goldston 2002); this variable opacity is closely tied to the fact that these stars are losing mass at a high rate ( $>10^{-7} M_{\odot}$  per year up to  $10^{-5} M_{\odot}$  per year) so the evolutionary status of Miras is that they are stars entering the final "superwind" (massive outflow) stage on the AGB (e.g. review Willson 2000). A number of stars initially classified as Miras are reclassified as SRb when their light curves develop irregularities, making the boundary between these two classes somewhat fuzzy. Similarly, most relatively regular carbon star LPVs have smaller amplitudes in the visual than do the oxygen-rich stars, and this may be telling us more about the sources of atmospheric opacity than about the evolutionary state, so that the SRa-Mira boundary is also fuzzy. Thus one interpretation would be that the asymmetry shows up when there is a sufficiently massive outflow to produce the large Mira amplitude for the oxygen-rich stars, and that the SR variables with asymmetries are those with different visual opacity but similarly massive outflows. Either the same mechanism leads to outflow and asymmetry (e.g. non-radial pulsation) or the outflow sets up conditions for asymmetry to be seen. In the first case, the non-radial structure originates at the photosphere; in the second, with aperiodicities in the outflow.

Most Miras are surrounded by translucent "molecular shells", a locus in the outflow where molecules and probably dust provide high local opacity, whose IR and visual optical depth is on the order of 1 (0.1 to several) - Perrin et al (2004). The physics of dust formation in the context of large-amplitude pulsation and consequent shocks is reviewed in Willson (2000). Dust grains nucleated in the refrigerated zone between shocks may require several pulsation cycles to grow to sufficient size to generate an outflow, and this would naturally lead to critical dust levels appearing in different cycles at different positions around the star. Whether by this or another mechanism, the translucent shell is likely to have a patchy opacity, allowing more of the photospheric light through in some places than in others. Thus a plausible explanation for the possibly universal asymmetry in Miras would be the formation of an inhomogeneous translucent molecular screen around 1.5 to 2.5 stellar radii.

In conclusion, we carried out a survey of AGB stars with the IOTA 3-telescope imaging interferometer at near-infrared wavelengths, searching for asymmetry in their flux distributions. We find that 29% of our sample show asymmetry. If we restrict the sample to only well resolved targets, then 75% of AGB stars, 100% of oxygen-rich Mira stars show asymmetry from our observations. On this basis, we hypothesize that all Mira stars might show detectable asymmetry if observed with adequate spatial resolution. The large frequency of asymmetry reported here suggests that angular size measurements and limb darkening studies of AGB stars carried out with 2-telescope optical long baseline interferometers should be interpreted with caution. We have initiated a systematic mapping program, namely, ‘The Mira Imaging Project’ funded by National Science Foundation (NSF) at the IOTA, ISI and VLBA interferometers to connect the asymmetry in space and time, and pin-point the mechanism(s) responsible for observed asymmetry.

This work was performed in part under contract with the Jet Propulsion Laboratory (JPL) through a Michelson Postdoctoral Fellowship to Ragland, funded by NASA as an element of the Navigator (planet finder) Program. JPL is managed for NASA by the California Institute of Technology. We acknowledge support from the NSF through research grants AST-0138303 and AST-0456047. The IOTA is principally supported by the Smithsonian Astrophysical Observatory and the Univ. of Massachusetts. The National Radio Astronomy Observatory (NRAO) is operated by Associated Universities Inc., under cooperative agreement with the NSF. We thank the referee for constructively critical comments that have helped us to significantly improve the paper. This research has made use of NASA’s Astrophysics Data System Bibliographic Services and AAVSO’s database for light curves.

## REFERENCES

- Allen, D. A. 1984, *Ap&SS*, 99, 101
- Baldwin, J. E., Beckett, M. G., Boysen, R. C., Burns, D., Buscher, D. F. et al. 1996, *A&A*, 306, 13L
- Belczyński, K., Mikołajewska, J., Munari, U., Ivison, R. J., & Friedjung, M. 2000, *A&AS*, 146, 407
- Berger, J.-P., Haguenaer, P., Kern, P., Rousselet-Perraut, K., Malbet, F., et al. 2004, *Interferometry for Optical Astronomy II*, Traub, W.A., Ed., Proc. SPIE 4838, 1099
- Blackman, E. G., Frank, A., Markiel, J. A., Thomas, J. H., & Van Horn, H. M. 2001, *Nature*, 409, 485

- Boothroyd, A. I. & Sackmann, I.-J. 1988, ApJ, 328, 632
- Bohme, D.D., 1978 AN, 299, 243
- Born, M. & Wolf, E. 1980, Principles of Optics, 6 edn. (Oxford, UK: Pergamon Press),  
Section 10.3.1
- Bowen, G. H. & Willson, L. A. 1991, ApJ, 375L, 53
- Brocksopp, C., Sokoloski, J. L., Kaiser, C., Richards, A. M., Muxlow, T. W. B. et al. 2004,  
MNRAS, 347, 430
- Chagnon, G., Mennesson, B., Perrin, G., Coudé du Foresto, V., Salomé, P. et al. 2002, AJ,  
124, 2821
- Cotton, W. D., Mennesson, B., Diamond, P. J., Perrin, G., Coudé du Foresto, V. et al. 2004,  
A&A, 414, 275
- Coudé du Foresto, V., Ridgway, S. & Mariotti, J.-M. 1997, A&AS, 121, 379
- Diamond, P.J. & Kembball, A.J., 2003, ApJ, 599, 1372
- Diamond, P.J., Kembball, A.J., Junor, W., Zensus, A., Benson, J. et al. 1994, ApJ, 430, L61
- Di Benedetto, G.P. 1993, A&A, 270, 315
- Dyck, H. M., van Belle, G. T. & Benson, J. A. 1996, 112, 294
- Dyck, H. M., Benson, J. A., van Belle, G. T. & Ridgway, S. T., 1996, AJ, 111, 1705
- Dyck, H. M., van Belle, G. T. & Thompson, R.R. 1998, 116, 981
- Frogel, J. A., Persson, S. E., & Cohen, J. G. 1981, ApJ, 246, 842
- Greenhill, L. J., Colomer, F., Moran, J. M., Backer, D. C., Danchi, W. C. et al. 1995, ApJ,  
449, 365
- Haniff, C. A., Ghez, A. M., Gorham, P. W., Kulkarni, S. R., Matthews, K. et al. 1992, AJ,  
103, 1662
- Hinkle, K. H., Scharlach, W. W. G., & Hall, D. N. B. 1984, ApJS, 56, 1
- Hofmann, K.-H., Balega, Y., Scholz, M. & Weigelt, G. 2000, A&A, 353, 1016
- Humphreys, E. M. L., Gray, M. D., Yates, J. A., Field, D., Bowen, G. H., & Diamond, P. J.  
2002, A&A, 386, 256

- Hutter, D. J., Johnston, K. J., Mozurkewich, D., Simon, R. S., Colavita, M. M. et al. 1989, *ApJ*, 340, 1103
- Imai, H., Obara, K., Diamond, P.J., Omodaka, T. & Sasao, T. 2002, *Nature*, 417, 829
- Jennison, R.C. 1958, *MNRAS*, 118, 276
- Knapp, G. R. & Morris, M. 1985, *ApJ*, 292, 640
- Karovska, M., Nisenson, P., Papaliolios, C. & Boyle, R.P. 1991, *ApJ*, 374, L51
- Karovska, M., Hack, W., Raymond, J. & Guinan, E. 1997, *ApJ*, 482, L175
- Kellogg, E., Pedelty, J. A. & Lyon, R. G. 2001, *ApJ*, 563L, 151
- Kraus, S. & Schloerb, F.P. 2004, *New Frontiers in Stellar Interferometry*, Traub, W.A., Ed., *Proc. SPIE* 5491, 56
- Lattanzi, M.G., Munari, U., Whitelock, P.A. & Feast, M.W. 1997, *ApJ*, 485, 328
- Luthardt, R. 1992, *Reviews of Modern Astronomy*, 5, 38
- Lopez, B., Danchi, W. C., Bester, M., Hale, D. D. S., Lipman, E. A. et al. 1997, *ApJ*, 488, 807
- Mastrodemos, N. & Morris, M. 1998, *ApJ*, 497, 303
- Mastrodemos, N. & Morris, M. 1999, *ApJ*, 523, 357
- Mennesson, B., Perrin, G., Chagnon, G., Foresto, V. Coude du, Ridgway, S. et al. 2002, *ApJ*, 579, 446
- Merrill, P.W., 1956, *PASP*, 68, 162
- Millan-Gabet, R., Pedretti, E., Monnier, J. D., Schloerb, F. P., Traub, W. A. et al. 2005, *ApJ*, 620, 961
- Monnier, J. D., Tuthill, P. G., Danchi, W. C. 2000, *ApJ*, 545, 957
- Monnier, J. D., Traub, W. A., Schloerb, F. P., Millan-Gabet, R., Berger, J.-P. et al. 2004a, *ApJ*, 602L, 57
- Monnier, J. D., Millan-Gabet, R., Tuthill, P. G., Traub, W. A., Carleton, N. P. et al. 2004b, *ApJ*, 605, 436

- Mozurkewich, D. & Armstrong, J.T. 1992, *High-Resolution Imaging by Interferometry II*, Beckers, J.M. and Merkle, F., eds. ESO Conference and Workshop Proceedings, **39**, 801
- Olofsson, H., Carlstrom, U., Eriksson, K., Gustafsson, B. & Willson, L. A. 1990, *A&A*, 230, L13
- Ostlie, D.A. & Cox, A.N. 1986, *ApJ*, 311, 864
- Pedretti, E., Millan-Gabet, R., Monnier, J. D., Traub, W. A., Carleton, N. P., Berger, J.-P., Lacasse, M. G., Schloerb, F. P., Brewer, M. K. 2004, *PASP*, 116, 377
- Pedretti, E. Traub, W.A., Monnier, J.D., Millan-Gabet, R.; Carleton, N.P., Schloerb, F.P., Brewer, M.K., Berger, J.-P., Lacasse, M.G., Ragland, S. 2005, *ApOpt.*, 44, 5173
- Perrin et al., Ridgway, S.T., Mennesson, B., Cotton, W.D., Woillez, J. et al., 2004, *A&A*, 426, 279
- Ragland, S., 1996, Ph.D. thesis, Physical Research Laboratory, India
- Ragland, S., Traub, W.A., Berger, J.-P., Millan-Gabet, R., Monnier, J.D. et al. 2004, *New Frontiers in Stellar Interferometry*, Traub, W.A., Ed., *Proc. SPIE* 5491, 1390
- Reid, M. J., Goldston, J. E., 2002, *ApJ*, 568, 931
- Richichi, A. & Calamai, G. 1993, *A&A*, 399, 275
- Richichi, A., Lisi, F. & Calamai, G. 1991, *A&A*, 241, 131
- Richichi, A., Chandrasekhar, T., Lisi, F., Howell, R. R., Meyer, C. et al. 1995, *A&A*, 301, 439
- Reimers, D. & Cassatella, A. 1985, *ApJ*, 297, 275
- Sahai, R., Morris, M., Knapp, G. R., Young, K. & Barnbaum, C., 2003, *Nature*, 426, 261
- Samus N.N., Durlevich O.V. et al. 2004, *Combined General Catalog of Variable Stars (GCVS4.2)*, Institute of Astronomy of Russian Academy of Sciences and Sternberg State Astronomical Institute of the Moscow State University
- Schwarzschild, M. 1975, *ApJ*, 195, 137
- Soker, N. & Zoabi, E. 2002, *MNRAS*, 329, 204
- Sokoloski, J. L. & Kenyon, S. J. 2003, *ApJ*, 584, 1021

- Soria-Ruiz, R., Alcolea, J., Colomer, F., Bujarrabal, V., Desmurs, J.-F. et al., 2004, *A&A*, 426, 131
- Struck, C., Cohanin, B. E. & Willson, L. A. 2004, *MNRAS*, 347, 173
- Su, K. Y. L. 2004, *ASP Conf. Ser. 313: Asymmetrical Planetary Nebulae III: Winds, Structure and the Thunderbird*, 247
- Sudol, J. J., Benson, J. A., Dyck, H. M., Scholz, M., 2002, *AJ*, 124, 3370
- Templeton, M.R., Mattei, J.A. & Willson, L.A. 2004, private communication
- Tuthill, P. G., Haniff, C. A. & Baldwin, J. E. 1997, *MNRAS*, 285, 529
- Tuthill, P. G., Haniff, C. A. & Baldwin, J. E. 1999, *MNRAS*, 306, 353
- Tuthill, P. G., Danchi, W. C., Hale, D. S., Monnier, J. D. & Townes, C. H. 2000, *ApJ*, 534, 907
- Traub, W.A., Berger, J.-P., Brewer, M.K., Carleton, N.P., Kern, P., et al. 2004, *New Frontiers in Stellar Interferometry*, Traub, W.A., Ed., *Proc. SPIE* 5491, 5491, 482
- Thompson, R.R., Creech-Eakman, M.J. & Akeson, R.L. 2002, *ApJ*, 570, 373
- van Belle, G. T. 1999, *PASP*, 111, 1515
- van Belle, G. T., Thompson, R. R. & Creech-Eakman, M. J., 2002, *AJ*, 124, 1706
- van Belle, G. T., Dyck, H. M., Thompson, R. R., Benson, J. A. & Kannappan, S. J. 1997, *AJ*, 114, 2150
- van Belle, G. T., Dyck, H. M., Benson, J. A. & Lacasse, M. G., 1996, *AJ*, 112, 2147
- Vassiliadis, E. & Wood, P. R. 1992, *Proceedings of the Astronomical Society of Australia*, 10, 30
- Weigelt, G. P. 1977, *Opt. Comm.*, 21, 55
- Weigelt, G., Balega, Y., Hofmann, K.-H. & Scholz, M. 1996, *A&A*, 316, L21
- Weiner, J., Tatebe, K., Hale, D. D. S., Townes, C. H., Monnier, J. D. et al. 2006, *ApJ*, 636, 1067
- Wesselink, A. J., Paranya, K. & de Vorkin, K., 1972, *A&AS*, 7, 257

Whitelock, P. A. 1987, *PASP*, 99, 573

Willson, L. A. 2000, *ARA&A*, 38, 573

Willson, L. A. & Kim, A. 2004, *ASP Conf. Ser.* 313: Asymmetrical Planetary Nebulae III: Winds, Structure and the Thunderbird, 394

Wilson, R.W., Baldwin, J.E., Buscher, D.F. & Warner, P.J. 1992, *MNRAS*, 257, 369

Wittkowski, M., Langer, N. & Weigelt, G. 1998, *A&A*, 340L, 39

Wood, B. E. & Karovska, M. 2004, *ApJ*, 601, 502

Wood, P. R. & Zarro, D. M. 1981, *ApJ*, 247, 247

Zuckerman, B. & Aller, L. H. 1986, *ApJ*, 301, 772